Article ID: 1000-324X(2017)11-1223-05 **DOI:** 10.15541/jim20170068

Interactions Between Bubble and Interface During $KTa_{1-x}Nb_xO_3$ Crystal Growth

LI Shu-Hui[1,2], PAN Xiu-Hong[1], LIU Yan[1], JIN Wei-Qing[1], ZHANG Ming-Hui[1], YU Jian-Ding[1], CHEN Kun[1], AI Fei[1]

(1. Shanghai Institute of Ceramics, Chinese Academy of Sciences, Shanghai 200050, China; 2. University of Chinese Academy of Sciences, Beijing 100039, China)

Abstract: The generation of bubbles and its interaction with the interface during melting and growth process of potassium tantalate niobate ($KTa_{1-x}Nb_xO_3$) crystals were visualized by a high temperature *in-situ* observation system. It was found that bubbles are generated mainly from the solid-liquid interface during melting, rather than from the melt. Bubbles with radii smaller than $0.7\bar{r}$ (where $\bar{r}$ is the mean radius of bubbles) arise mostly from nucleation at the interface while radii larger than $1.5\bar{r}$ are the result of coalescence. The existence of the bubble not only lowers the growth velocity of the near interface, but also affects the structure of the crystal. The effect of a bubble on the growing interface depends on their dimension ratio together with the moving speed of the interface. There are three typical kinds (hat-, sphere- and ellipsoid-shaped) of vapor inclusion morphologies being demonstrated. The analysis of the bubble behavior can promote the understanding of the formation of inclusion defects in KTN crystal growth process.

Key words: potassium tantalate niobate; crystal growth; bubble; *in situ* observation; computed tomography

Potassium tantalate niobate, $KTa_{1-x}Nb_xO_3$(KTN), which has the largest quadratic electro-optic effect, is one of the earliest discovered materials with photorefractive characteristics[1-2]. It has attracted much attention as a promising material for electro-optical applications in the past few years[3-5]. Although the unparalleled properties of KTN single crystals have been realized for more than half century[1,6-7], application is still extremely limited because of the rigorous growth conditions[2,6]. In order to find a relatively simply way to obtain KTN crystal, researchers have tried several methods[8-10]. But some growth defects, such as inclusion, crack and striation, still restrict the application of the crystal[11-13]. With the purpose of obtaining KTN single crystal with high quality, it is imperative to strength the study on its growth defects[12]. However, due to the difficulty for real-time observation in a high temperature environment, few studies have been focused on the generation procedure of inclusions during KTN crystal growth from the melt. In this work, we try to study the generation of bubbles with the help of a high temperature *in-situ* observation system[14-18]. Furthermore, combined with the morphological analysis of bubbles-induced inclusions, the influence of the existing bubble on the crystal structure was discussed in detail.

1 Experiments

$KTa_{1-x}Nb_xO_3$ crystals with x = 0.78 were obtained in a melt growth apparatus, then the melting and growth process were performed and visualized in a high temperature *in-situ* observation system. The system was comprised of a heating chamber and a loop-shaped Pt wire heater as shown in Fig. 1. The Pt wire (Φ 0.2 mm) as shown in Fig. 1(a) was employed to heat and suspend the melt during the *in-situ* observation experiment of crystals with high melting points. The inner diameter of the loop is ~1.20 mm. Pt-10% Rh thermocouple (Φ 0.08 mm) as shown in Fig. 1(b) located in one side of the loop is used to measure the temperature with the fluctuations of less than ±2℃ above 1000℃. The power was applied to both the electrodes of the wire as shown in Fig. 1(c) and 1(d). The video of the crystal growth process was recorded from the microscope by a camera.

A typical experimental procedure was carried out in the following way. Before each test, the amount of the test melt was precisely controlled until a thin transmissive flat film of about 300 μm thickness in the center of the loop-shaped heater was obtained. Turn on the power source, record the temperature as the melting temperature

Received date: 2017-02-14; **Modified date:** 2017-05-15
Foundation item: National Natural Science Foundation of China (51472263, 51602330); Shanghai Sailing Program (16YF1413100)
Biography: LI Shu-Hui (1992–), female, candidate of master degree. E-mail: lishuhui@student.sic.ac.cn
Corresponding author: LIU Yan, professor. E-mail: liuyan@mail.sic.ac.cn; PAN Xiu-Hong, associate professor. E-mail: xhpan@mail.sic.ac.cn

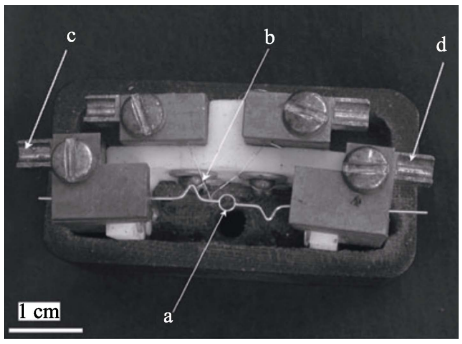

Fig. 1 The photo of the growth cell
(a) Pt wire heater, (b) Pt-10% Rh thermocouple, (c) and (d) are electrodes

T_m when the crystal edge began to melt. Continue to heat until the crystal was melted completely. Maintain at that temperature for at least five minutes to obtain the stable melt system. Bubbles would continue merging until there was only one bubble in the melt during this process, then cool the system to 20 K below T_m. Touch the melt by a Platinum wire (Φ 0.2 mm) and there would be a small crystal. The crystal was growing up in this under- cooled environment and touching the bubble. The whole process was recorded by CCD until the system was cooled to room temperature. After that, a Three-dimensional Computed Tomography (3D CT) Test was determined by Microfocus X-ray three-dimensional perspective system (Y. Cheetah) in order to analyze bubbles' distribution in the as-grown crystals.

2 Results and Discussion

2.1 Bubble generation process

Bubble generation process occurred mostly during the heating process owing to the poor compactness of crystals. The gas in the initial crystal may form the contents of the bubbles. Figure 2 shows the typical time series of pictures taken while the crystal was melted. At the initial stage of heating, the crystal melts along the edges firstly with no bubbles observed as shown in Figure 2(a). However, some bubbles, numbered 1#, 2# and 3# in Figure 2(b), nucleated at the Solid-Liquid (S-L) interface, staying for a short time and then moving to the margin under the convection in the melt[15,19]. The initial sizes of bubbles are usually smaller than 25 μm, but they merge extremely fast. It has been calculated that the time needed for coalescence of two bubbles is less than 0.01 s. Unfortunately, our equipment is not sophisticated enough to capture the details of bubbles' movement in such a tiny time. Continue heating and the crystal melts slowly. More bubbles generate and grow from the S-L interface ceaselessly as shown in Figure 2(c). What should be noted is that bubble coalescence process can occur not only in the process of movement, but also during the generation process. Bubble 1# in Figure 2(c) shows the merged result of bubble 1#, 2# and 3# in Figure 2(b). When the crystal completely melts, the distribution among bubbles' size has the characteristics of polarization. Figure 2(d) shows this phenomenon. Bubbles in the center are small. They are just produced from the melting process and the next moment they are about to merge and move to the edge. On the other hand, there are some bigger bubbles located on the margin of the loop. They are made by the coalescence process of bubbles generated before. Eventually, there are only several big bubbles in the melt after a few seconds. It turned out that bubbles with radii smaller than $0.7\bar{r}$ (where $\bar{r}$ is the mean radius of the bubbles) are mostly formed through nucleation during melting process while radii larger than $1.5\bar{r}$ are the result of coalescence. During the whole process of melting, no bubbles were found to form from the melt. They are mostly generated from the S-L interface. This phenomenon is different with the bubble growth in rhyodacitic melt, in which the bubble nucleated in the melt, rather than at the interface[20].

2.2 Effect of bubbles with growing solid- liquid interface

The interaction of bubbles with the growing S-L interface is important since it has significant effect on the as-grown crystal structure. Figure 3 shows a typical interacting process during KTN crystal growth. Observation provided by Figure 3(a) shows that one spherical bubble with the diameter ~140 μm appears on the margin of the melt at t = 6.90 s. A small KTN crystal is nucleated and the S-L interface is relatively flat. Here, the moment the

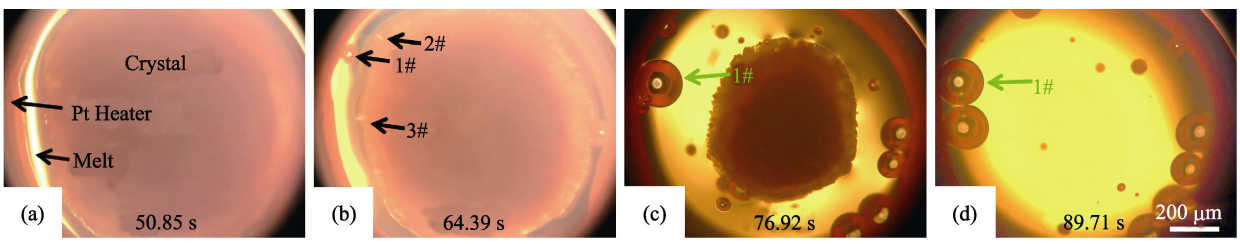

Fig. 2 Bubble behaviors during melting process (10 ×)
The moment the crystal began to melt is defined as t = 0 s

crystal began to crystalized is defined as t = 0 s. Comparing to Figure 3(a), Figure 3(b) at t = 21.00 s indicates that remaining the shape unchanged, both the radius of the bubble and the size of the crystal increase with time due to smaller solubility[21] and larger undercooling, respectively. After about two seconds, the S-L interface reaches with the bubble wall. As the sustained growth of the interface, the bubble becomes ellipsoidal firstly under the extrusion of the interface as shown in Figure 3(d)-(e). Due to the effect of surface tension, the bubble will not break. And then the bubble was captured into the solid crystal with S-L interface moving continuously as shown in Figure 3(f). As a result, there is a vapor inclusion caused by the bubble in the as-grown KTN crystal. It is found that the existence of the bubble will make the velocity of the interface lowered over one half, which can be explained by the strong radiation heat transfer process at high temperature on the solidification front[22]. Then a groove- shaped structure appears in this area, which seriously affect the quality of crystals[12-13].

2.3 X-ray CT analysis of bubble-induced inclusion

In-situ observation system can reflect the interactions between bubbles and the interface clearly. However, it can only show information in two-dimensional plane. X-ray computed tomography (CT) imaging is a nondestructive testing technology which can show the shape and size of the subject in a three-dimensional perspective[23]. Figure 4(a)-(c) show the Micro focus 3-D X-ray imaging results of the sample in Figure 3 after cooling to ambient temperature. They are front view, left view and top view in the inclusion's position, respectively. Here the black areas represent the gas phase. Three rectangles represent the shape features area under corresponding perspective. During the above process, the length of the interface L is much larger than the diameter of the bubble D. The length to the diameter ratio is 2.6 when the bubble

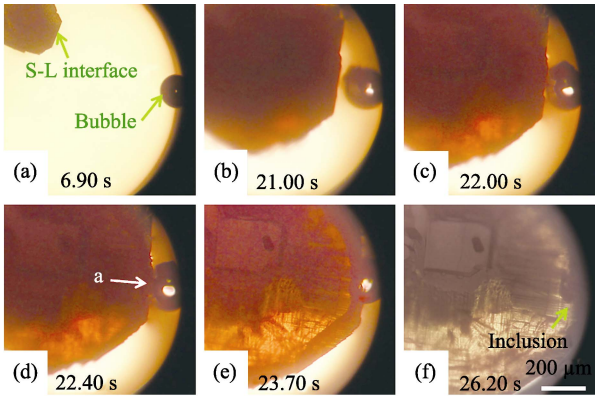

Fig. 3　Interaction process between small single bubble and large S-L interface (20 ×)
The moment the crystal began to crystalized is defined as t = 0 s

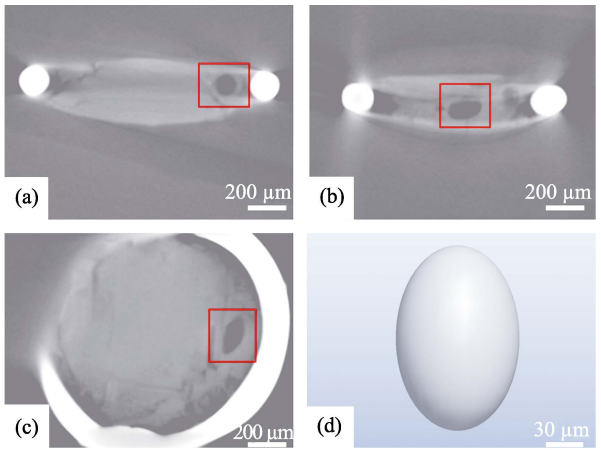

Fig. 4　Three views and stereo image of an inclusion
L/D = 2.6, v_0 = 87 μm/s

interacts with the growing S-L interface, which is greater than 1 as shown in the picture. According to the three orthographic views of the inclusion, we determine the stereoscopic graph as shown in Figure 4(d). It is an ellipsoid- shaped inclusion. In general, when L/D > 1 and the interface front moves fast, the bubble will be pressed into ellipsoid.

When it comes to a much smaller velocity of the interface front, the influence of the bubble on the crystal will be different. Here is one case with the length to the diameter ratio is about 1.3, and the movement speed of the interface v_0 is ~23 μm/s. When the interface contacts with the bubble, the moving velocity slows down to 10 μm/s due to the weakened radiation heat transfer process as we have discussed before. Unlike the circumstance of fast moving front as shown in Figure 3, the bubble maintains the sphere shape in the whole process during the bubble and the S-L interface interaction. After the system is completely cooling down, the shape of the bubble remain the same and it grows into the crystal completely. Figure 5(a)-(c) show three views of the inclusion in this circumstance. It is still in a spherical shape

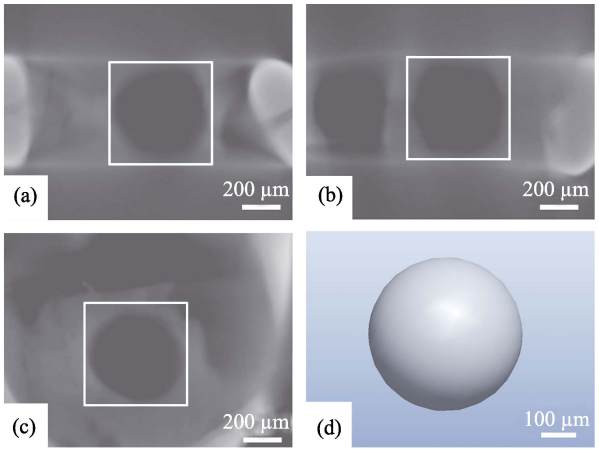

Fig. 5　Three views and stereo image of an inclusion
L/D =1.3, v_0 = 23 μm/s

(Figure 5(d)). As a result, when the diameter of the single bubble is smaller than the size of the interface whose moving speed is relatively small, the bubble will embed in the crystal with original sphere shape.

Another situation occurs when the dimension of the interface is smaller than the diameter of the bubble, namely $L/D < 1$. For example, a small KTN crystal whose length is 100 μm contacts with a bubble whose diameter is 180 μm near the edge of the heater. Here, the length ratio is $L/D \sim 0.6$. In this case, the tiny crystal will extrude the bubble. Then the bubble section which contacts with the crystal forms a depression structure under the extrusion force. The depression size grows with the time. Eventually, it forms a hat-shaped structure as shown in Figure 6. The external diameter of the inclusion is 200 μm, which is larger than the diameter of the bubble. In contrast, the height of the inclusion is only 120 μm. The size distribution indicates that the bubble is squeezed along the direction of crystal growth. But on the direction parallel to the interface, bubble size increases. In short, when the length of the interface is smaller than the diameter of the bubble, the shape of the bubble-induced inclusion in the as-grown crystal will be hat-shaped.

It should be noted that, in an extremely case, that the interface grows quickly with velocity v_0 over 1.0 mm/s, the bubble will collapse and disappear during the interaction process. As a result, no obvious bubble inclusion can be found in the as-grown crystal.

3 Conclusions

In the present work, the behaviors of the bubble during melting and growth process of KTN crystal were observed. It was found that bubbles prefer to generate mainly from the solid-liquid interface, rather than from the melt. Then they merged and moved during the whole melting process. Only a few large bubbles were left on the margin of the loop in the melt eventually. The bubble makes the near region growing at a slower velocity, usually less than half of the average velocity. The effect of single bubble on the crystal growth depends on not only their dimension ratio, but also moving speed of the interface. When the crystal size is smaller than the diameter of the bubble, the bubble will become a hat-shaped inclusion in the as-grown crystal. When the bubble is smaller than the interface, the shape of the inclusion depends on the interface moving speed. There will be a spherical inclusion with a slow speed, while an ellipsoidal inclusion will be produced when the interface moves relatively fast. Depending on the shape of the inclusion, the growth factors, such as the moving velocity at different positions during the crystal growth process can be deduced.

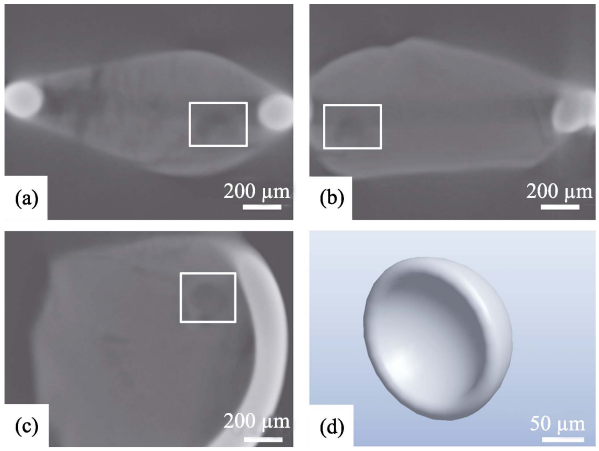

Fig. 6 Three views and stereo image of an inclusion
$L/D = 0.6$, $v_0 = 9$ μm/s

References:

[1] CHEN F S, EUSIC J E, KURTZ S K, *et al*. Light modulation and beam deflection with potassium tantalate-niobate crystals. *J. Appl. Phys.*, 1966, **37(1):** 388–398.

[2] WANG J Y, GUAN Q C, WEI J Q, *et al.* Growth and characterization of cubic $KTa_{1-x}Nb_xO_3$ crystals. *J. Cryst. Growth*, 1992, **116:** 27–36.

[3] SASAURA M, IMAI T, KOHDA H, *et al.* TSSG pulling and LPE growth of $KTa_{1-x}Nb_xO_3$ for optical waveguides. *J. Cryst. Growth*, 2005, **275:** e2099–e2103.

[4] SHINAGAWA M, KOBAYASHI J, YAGI S, *et al.* Sensitive electro-optic sensor using $KTa_{1-x}Nb_xO_3$ crystal. *Sens. Actuators A*, 2013, **192:** 42–48.

[5] OHMI M, FUKUDA A, MIYAZU J, *et al.* Development of novel high-speed en face optical coherence tomography system using KTN optical beam deflector. *Appl. Phys. Express*, 2015, **8:** 027001.

[6] RYTZ D, SCHEEL H J. Crystal growth of $KTa_{1-x}Nb_xO_3$ ($0<x\leqslant 0.04$) solid solutions by a slow-cooling method. *J. Cryst. Growth*, 1982, **59:** 468–484.

[7] KUGEL G E, MESLI H, FONTANA M D. Experimental and theoretical study of the Raman spectrum in $KTa_{1-x}Nb_xO_3$ solid solutions. *Phys. Rev. B*, 1988, **37(10):** 5619–5628.

[8] WHIPPS P W. Growth of high-quality crystals of KTN. *J. Cryst. Growth*, 1972, **12:** 120–124.

[9] IMAI T, YAGI S, SUGIYAMA Y, *et al*. Growth of potassium tantalate niobate single crystal fibers by the laser-heated pedestal growth method assisted by a crystal cooling technique. *J. Cryst. Growth*, 1995, **147:** 350–354.

[10] WANG X P, LIU B, YANG Y G, *et al*. Growth of KTN crystals by double crucible Czochralski method. *Mater. Res. Innovations*, 2014, **18(5):** 334–339.

[11] ILANGOVAN R, BALAKUMAR S, SUBRAMANIAN C, *et al*. Growth and characterization of $KTa_{0.3}Nb_{0.7}O_3$ single crystals. *Mater. Chem. Phys*., 1993, **36:** 174–176.

[12] WANG X P, WANG J Y, WU J, *et al*. Growth defects in cubic $KTa_{1-x}Nb_xO_3$ crystal. *Chinese J. Struct. Chem.*, 2008, **27(3):** 261–266.

[13] WANG X P, WANG J Y, YU Y G, *et al*. Cubic $KTa_{1-x}Nb_xO_3$ crystal growth by Czochraski method. *Chinese J. Rare Metals*, 2006, **30(6):** 841–845.

[14] LIU Z H, JIN W Q, PAN Z L, *et al*. Experiment and numerical

simulation of velocity and temperature fields in $KNbO_3$ solution. *J. Inorg. Mater.*, 2002, **17(6):** 1112–1116.

[15] PAN X H, JIN W Q, AI F, *et al*. Effect of surface-tension driven convection on interfacial boundary layer during BaB_2O_4 single crystal growth. *J. Inorg. Mater.*, 2007, **22(6):** 1239–1242.

[16] LIANG X A, JIN W Q, PAN Z L, *et al*. Study on $Bi_{12}SiO_{20}$ melt Marangoni convection. *J. Inorg. Mater.*, 2001, **16(1):** 32–36.

[17] HONG Y, JIN W Q, PAN X H. Thermalcapillary convection in $NaBi(WO_4)$ melt. *Chin. Phys. Lett.*, 2004, **21(10):** 1986–1988.

[18] HONG Y, JIN W Q, PAN X H, *et al*. *In situ* observation of dendrite in $Pb_5Ge_3O_{11}$ crystal growth. *J. Inorg. Mater.*, 2006, **21(2):** 335–338.

[19] PAN X H, JIN W Q, LIU Y, *et al*. Effect of surface tension-driven flow on BaB_2O_4 crystal growth from high temperature melt-solution. *Cryst. Res. Technol.*, 2008, **43(2):** 152–156.

[20] MASOTTA M, NI H, KEPPLER H. *In situ* observations of bubble growth in basaltic, andesitic and rhyodacitic melts. *Contrib. Mineral. Petrol*, 2014, **167(2):** 1–14.

[21] PAPALE P. Modeling of the solubility of a one-component H_2O or CO_2 fluid in silicate liquids. *Contrib. Mineral. Petrol.*, 1997, **126:** 237–251.

[22] YAO T, HAN J C, ZUO H B, *et al*. Bubble formation in sapphire single crystals. *J. Inorg. Mater.*, 2008, **23(2):** 439–442.

[23] URUSHIHARA Y, HASEGAWA H, IWASAKI N. X-ray micro-CT observation of the apical skeleton of Japanese white coral coral-lium konojoi. *J. Exp. Mar. Biol. Ecol.*, 2016, **475:** 124–128.

$KTa_{1-x}Nb_xO_3$ 晶体生长过程中气泡与界面的相互作用

李淑慧[1,2], 潘秀红[1], 刘　岩[1], 金蔚青[1], 张明辉[1], 余建定[1], 陈　锟[1], 艾　飞

(1. 中国科学院 上海硅酸盐研究所, 上海 200050; 2. 中国科学院大学, 北京 100039)

摘 要: 本研究通过高温实时观察系统可视化研究了钽铌酸钾晶体的熔化和生长过程中气泡的产生及其与界面的相互作用。研究发现气泡在熔化过程中主要从固液界面处而不是熔体中产生。半径小于 $0.7\bar{r}$ (其中 $\bar{r}$ 为气泡平均半径)的气泡大多来源于在固液界面处的成核, 而半径大于 $1.5\bar{r}$ 的气泡则为多个小气泡合并的结果。气泡的存在不仅会使临近界面生长速度降低, 还会影响晶体结构。单个气泡对生长界面的影响不仅取决于二者的长度比例, 还取决于界面的移动速度。实验证明了三种典型的包裹体结构(帽子状、球状以及椭球状)。本文对于气泡行为的研究有助于了解 KTN 晶体生长过程中包裹体的形成过程。

关　键　词: 钽铌酸钾; 晶体生长; 气泡; 实时观察; CT

中图分类号: O781　　**文献标识码:** A